Eur. Phys. J. Special Topics **177**, 83–101 (2009)

DOI: 10.1140/epjst/e2009-01169-4

THE EUROPEAN PHYSICAL JOURNAL SPECIAL TOPICS

Regular Article

The role of homophase and heterophase interfaces on transport properties in structured materials

S. Gemming[1,a], T. Kunze[1], K. Morawetz[1,2], V. Pankoke[1], R. Luschtinetz[3], and G. Seifert[3]

[1] FZ Dresden-Rossendorf, PO Box 510119, 01314 Dresden, Germany
[2] International Center for Condensed Matter Physics, 70904-910 Brasilia, Brazil
[3] Physikalische Chemie, TU Dresden, 01062 Dresden, Germany

Abstract. In structured or self-organized materials spatial confinement effects lead to structure- and interface-controlled modifications of the bulk transport properties. In part, such modifications can be accounted for by a classical master equation approach for the transport of the different charge carrier species. The rather large quantity of parameters, which enter such an approach, can more or less easily be adjusted to the dimensional characteristics, local potential changes at interfaces, and the electronic settings of the system as well as to temperature effects. On the other hand, a microscopically more detailed and mostly parameter-free picture is obtained from a quantum-mechanical treatment on the basis of the density-functional theory. An extension by a Green's function formalism allows the determination and analysis of electronic transport through contacted nanostructures. Examples will be given to demonstrate the applicability of the different approaches for dissipative and hopping transport through a regular array of nanostructures, for a mechanically triggered metal-insulator transition in nanowires, and for the enhanced conductivity at multiferroic domain walls.

1 Introduction

Recent achievements in experimental techniques for the targeted preparation, analysis and manipulation of nanoscale elements for functional devices have inspired both experimental and theoretical efforts to quantify the electronic transport through junctions of nanometer-sized dimensions and to study the integration of such systems into larger units. Such a complex task requires modeling at length scales which range from picometer resolution for the calculation of basic electronic properties by first-principles and ab-initio methods up to the simulation of complete and operating devices by classical rate equation approaches for transport on the micrometer scale.

For simple and uniform systems a large variety of theoretical methods has been established to study the transport microscopically. To name a few examples – an analysis of the band dispersion and the density of electronic states obtained by density-functional calculations (DFT) yields insight in the propensity of nanowires or tubes towards ballistic conductance [1–6] and the changes introduced by defects [7–10], dopants [11–14], and alloying [15–18] or in the extrinsic conductivity induced in semiconductors by electrically, even magnetically active dopants, [10,13,19–22] and density-functional perturbation theory may be employed to calculate local polarizations which give rise to electronically active space charge regions [23–34]. The single-particle orbitals obtained by such an approach may further be introduced into a Landauer-type expression for the conductivity in terms of a matrix Green's function (GF) [21,35–41], and

[a] e-mail: s.gemming@fzd.de

a more sophisticated treatment allows the calculation of current and conductivity by non-equilibrium GF employing molecular states [42–73]. Also spin transport has been addressed successfully within that framework. Recent examples for that include the modification of electronic transport in wires by magnetic impurities [4,35,37,38] or the spin filter effect of metallic nanowires or interfaces [74–78]. Even correlation effects for conduction at interfaces have been included either in a mean-field manner [79,80] or by employing correlated molecular states with a multireference or a scattering approach to transport [81–83] or into quantum master equations (MEs, for a thorough comparison with the density-functional-derived methods, see ref. [83]). Common to all these approaches is their high level of detail, which impedes the routine study of all but small or perfectly periodic systems.

For this reason, the study of transport in larger and more realistic, still nanostructured devices relies on simulations with simplified models, which employ a set of device-specific material parameters. Classical analytical approaches allow the simulation of device characteristics in the ballistic conductance regime [84,85], or the derivation of ballistic correction terms for modeling conductors with disorder-driven weak electron localization [86,87]. For systems perturbed by a more pronounced structural flexibility or in more strongly disordered, doped or defective conductors, electronic transport may switch from an ideally loss-less ballistic regime conveyed by delocalized states to a tunneling transport between strongly localized states [88–90]. Transitions of Kosterless-Thouless [91] Wigner [92,93] or Anderson-type [89,94–97], have recently been reported, and evidence was given that the transition type can also vary with changing structural features of investigated system [93,98]. If the degree of perturbation or its dimensionality can be smoothly adjusted, also intermediate transport regimes may be achieved and described by e.g. assuming diffusive transport [22,99] or by variable-range hopping simulations [100,101] and numerical investigations on the transition between such regimes [102–104]. For benchmarking a numerical formalism, however, a more uniform reference system is suited better, thus the present review will focus only on the limiting cases, the ballistic conductance introduced above and the tunneling transport between localized states. Especially approaches for the strongly localized regime have been shown to contribute significantly to a better understanding of electronic conductance through arrays of quantum dots [105–111] ordered molecule arrays with spatially separated local electronic states [112–115] or along molecules with electronically separated fragments [116–120] and even more extended junction geometries with bound and quasi-bound states [40,121–125]. Transport through such a series of localized states may be achieved by electron tunneling as basic process of the so-called 'hopping' conductance, a concept, which was first introduced to descibe the transport of charge carriers between electrically active defect sites in an insulator [126]. Simplified tight-binding GF schemes have, for instance, been invoked to separate the different hopping processes that contribute to electron transfer along DNA strands [127–132] or to investigate electronic and thermal conductance through self-assembled layers of organic molecules [114,115]. In the classical limit, balance equations can be employed to simulate transport through localized states provided that the mobility law is given by experiment [133,134].

For analytical as well as applicative purposes such nanostructured elements have to be incorporated into a larger setup via contacts, through which a bias can be applied. Especially in molecular electronics, where the interfaces between molecule and leads comprise a large part of the device, the contact issue is decisive, hence it has incited numerous investigations, recently [135–144]. Figure 1 depicts the typical setup encountered in such investigations. If the central, nano-sized part of the structure may be regarded as a more meso-scale 'black-box' device with given current-voltage characteristics and bias dependence of the transport, then a standard continuum approach is very well capable of simulating the electrical behavior of a more complex circuitry. However, if the central structure becomes a nanoscale object, quantum-size effects come into play and a quantum mechanical treatment is required to treat the influence of such effects on the carrier transport properly. And finally, the presence of the interfaces created upon contacting may again substantially alter the properties of the whole device. Only if the contacts were electronically 'transparent', the transport would ideally be determined by the internal electronic structure of the central region. In realistic systems, however, the contact has a specific atomistic and electronic structure, which deviates from both the bulk properties

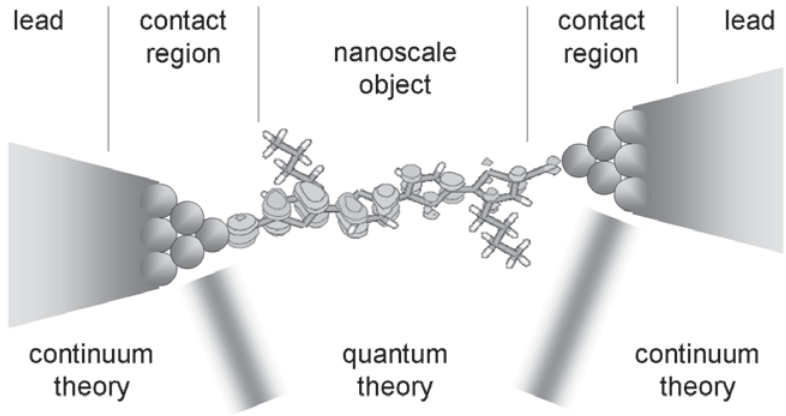

Fig. 1. Schematic representation of a nano-sized electronically active element embedded in a large-scale circuitry. Gray shaded areas in the diagram indicate the crossover between regions which require quantum mechanical or continuum theoretical treatment. Special focus is on the contact region, which requires a microscopic and quantum-based treatment if the contact is not ideally electronically transparent.

of the lead material and the local cluster or molecular properties of the gateable central structure.

A single technique is hence not capable of describing all aspects appropriately, thus a stringent multi-scale treatment is required, which accounts for transport across the contact interfaces and along larger unperturbed patches with equal accuracy. Recent progress for e.g. simulating thermal or electronic conductance across a sequence of different materials within a nanostructured transistor [145–148] underlines the viability of multi-scale, especially parameter-transfer-based methods to phenomena determined by the presence of interfaces.

The present contribution aims at showing how such a simulation scheme can be realized for the simulation of electronic conductivity by suitably interfacing established theoretical methods. First-principles calculations with high spatial resolution are the established first choice to elucidate the changes of the local electronic and magnetic structure at metal-metal, metal-semiconductor or metal-insulator interfaces. Parameters obtained from such calculations, e.g. of the central part and the contact region indicated in Fig. 1 may then be inserted into a more approximate microscopic ansatz or into a classical formulation for the leads. In this way, quite sophisticated, realistic multilayer systems can be treated theoretically by balance equations and subjected to different operating conditions, including external electric fields.

The present contribution is structured as follows: an overview of different charge transfer mechanisms is given in Section 2, quantum-mechanics-based and classical methods for the different conduction types are introduced in more detail in sections 3 and 4 along with the combination to a quantum-mechanics-based classical description of transport in an organic field-effect transistor with ferroelectric gating, and open questions and challenges are discussed in the final section.

2 Mechanisms of electron transfer

Early theoretical studies focused on the electron redistribution which occurs within a confined system upon excitation of an intrinsic electron from an occupied to an unoccupied level or upon extrinsically triggered changes of the total electron number during redox processes. Such perturbations of the ground state electronic structure are followed by a relaxation of the electron system, and it has been controversially discussed, which type of pathway is favored during the involved charge redistributions (for a recent comparative study see e.g. ref. [149] and refs. within). Both experimental and theoretical efforts focused on synthesizing and characterizing molecular

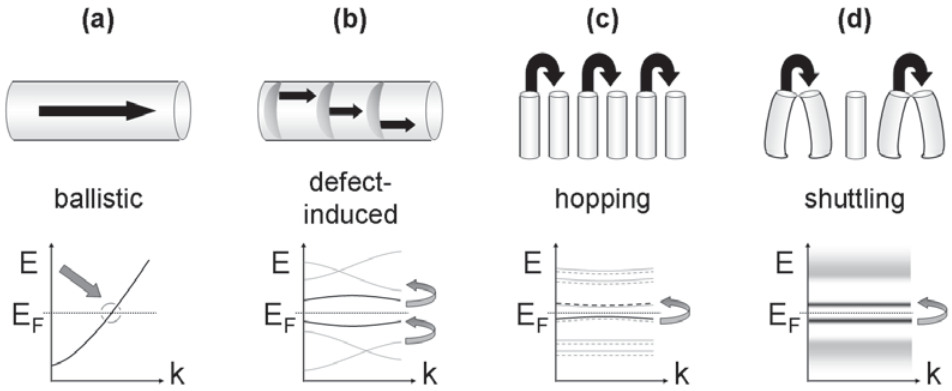

Fig. 2. Schematic representation of the structural and electronic characteristics of the four transport mechanisms discussed in the present manuscript: (a) ballistic, (b) dopant- and/or defect-induced, (c) hopping, and (d) shuttling transport. The upper part of the panels sketches prototypical geometries of nanoscale objects, which exhibit the specific conduction mechanism, the lower part visualizes the electron level structure as a function of the reciprocal space vector k. States actively involved in the specific conduction mechanism are denoted by black lines, other states are dark grey. For the abscissa k is chosen here, because it reflects the degree of spatial localization of the electronic states. Metallic (a) and semiconducting (b) materials have delocalized states with noticeable dispersion, whereas the separate molecules or molecular fragments in (c) and (d) contain strongly localized ones (states which stem from adjacent molecules are distinguished by solid and broken lines). In case (d) the vibration-induced broadening of the electronic levels is indicated by giving shaded areas instead of sharp levels.

test systems which allow for a competition of electron transfer "through bond" and "through space". This concept distinguishes intramolecular interactions into those determined by a direct spatial overlap of the two involved local fragment orbitals ("through space") and those where the no direct overlap is possible. In the latter case the interaction is transferred "though bond" via delocalization over the orbitals of intermediate fragments and can overcome quite considerable distances [150,151].

A prominent example is the enzymatic repair of DNA strands damaged by UV irradiation, which attracted widespread attention over the last two decades. Early investigations invoked qualitative linear energy transfer considerations with simplifying model parameters [152] or structurally based similarity measures [153] to determine the probability to form non-Watson-Crick base pairs. Later, extensive studies by semiempirical quantum mechanics [154,155], by density-functional theory [156,157], or by combined ab-initio and molecular mechanics calculations [158–161] yielded insight in the underlying orbital structure, which leads to light-induced dimerization of bases and in the electron transfer required to break, i.e. 'repair' such defects. Recent investigations, which focus on the transfer properties of DNA, employ multi-scale approaches, e.g. to quantify key transfer steps by coupling quantum mechanics for the electronically active region to molecular modeling with empirical potentials for the chemical environment [162], or to include thermal effects on the transport in Monte-Carlo simulations to apply Marcus' theory on a set of structures obtained from molecular dynamics [163]. As such intramolecular excitation-relaxation processes are out of the scope of the present discussion the reader is referred to recent review articles [164,165] for more details on the theoretical description.

For systems subjected to an external electric bias the through-space-through-bond concept of intramolecular electron transfer must be generalized to the presence and dynamics of external charge carriers. Following standard classification schemes, four major transport mechanisms may be distinguished and arranged in increasing order of spatial electron localization: Conduction may be of (a) ballistic, (b) dopant- or defect-induced, (c) hopping or (d) shuttling type. The upper row of Fig. 2 depicts schematically the dominating mechanisms which determine the transfer pathway, the lower panels sketch the corresponding electronic structure.

In systems with ideal metallic conductivity, sketched here as wire structure in panel (a), electrons may be transferred in a loss-less manner if the length of the structure is less than the mean free path for electrons. As the material-dependent values of the mean free path may range up to tens or hundreds of Ångstrom, nanostructured materials meet the geometric criterion for ballistic conductance. The electronic structure of such systems is characterized by energy bands with a more or less ideally parabolic dispersion in reciprocal (k) space (in an ideal free electron gas the band dispersion is parabolic, because in the absence of a confining or scattering potential only the kinetic energy term k^2 remains). In a metal, one or more bands intersect the Fermi level, E_F, as indicated by the circle in panel (a). Such bands are only partially occupied by electrons (below E_F) and mediate the intrinsic metallic mobility within or along the nanostructure. Here, structural defects, compositional imperfections or strains, which may occur close to the contacts to external wiring during the integration into a larger structure very likely provide additional scattering centers. Hence, such deviations from the ideal geometry will usually reduce the electron mean free path, and be detrimental for ballistic transport. Another aspect is that the conductance properties of the macroscopic leads may dominate the transport observed across the device, especially for metallic wires or tubes. This effect is less pronounced in molecular electronics, where a single molecule or cluster with well-defined, dispersion-free electronic states is bonded to metallic contacts (see Fig. 1), e.g. in a break junction geometry. Typical molecular dimensions are below the mean free path in classical metals, but above distances which can be overcome significantly by Fowler-Nordheim tunneling. Therefore, modeling strategies for case (a) are also applicable to several challenges in molecular electronics.

Semiconductors have a small energy gap between occupied and unoccupied electronic states, hence they can also exhibit intrinsic electronic transport, if electrons are excited from the valence band (dark grey lines below E_F) to the conduction band (dark grey lines above E_F). This effect can greatly be enhanced by electronically active dopants which provide additional states within the band gap (dark lines). In contrast to the states of the host crystal, such dopant levels are more strongly localized in the vicinity of the dopant atom, thus they have no or little dispersion. In doped semiconductors, both electrons and holes can contribute to the conduction. Electron-rich atoms with filled levels, that are energetically close to the conduction band can donate such electrons into the conduction band. In this way the electrons formerly localized on the dopant enters the delocalized states of the conduction band and provide a current of negatively charged carriers (n-type doping). In an analogous form, positive charge carriers, holes, are introduced into the valence band, if an electron-poor dopant can localize electrons, that formerly occupied delocalized states of the semiconductor (p-type doping). In contrast to case (a), local structural defects such as the dopants enhance the conductivity. Nevertheless, integration into larger devices with metallic leads is also not trivial, because the work functions and the positions of the Fermi levels in device and lead have to match. Furthermore, binary or ternary phases may be formed if the interface is reactive, and the transport is then modified by the electronic properties of the additional phase.

A hopping- or tunneling-type conductivity can be achieved for rather close-packed arrays of systems with localized electronic states, separated by a moderate tunnel barrier. For the present discussion, which focuses on the integration of flexible molecules into organic-inorganic devices, panel (c) is limited to a regular, parallel arrangement of π-stacked aromatic molecules, but similar arguments hold also for transport through series of clusters, particles or embedded quantum well structures. In the off state of such an arrangement, all levels are energetically degenerate, but spatially separated. Panel (c) visualizes a simplified case with levels from only two molecules, denoted by solid and dashed lines. Without an external potential difference a weak intrinsic carrier density may be achieved, e.g. by illumination of dye compounds. After photoexcitation of an electron from the highest occupied molecular orbital (HOMO) to the lowest unoccupied molecular orbital (LUMO) the electron most probably recombines with the hole in the HOMO. The carriers may, however, also tunnel to adjacent molecules and contribute to a photocurrent. As in doped semiconductors, the mobile carriers can be of both electron- and hole-type. If an external bias is applied, the molecular levels are shifted with respect to each other and photoinduced electrons and holes tunnel in different directions. Typically different mobilities are obtained for electrons and holes, because already the spatial overlap between HOMO states is different from the one of the LUMO states, thus also the tunnel barriers differ.

Commonly, however, carriers that are are transported along the level cascade have been injected by applying a bias voltage at external electrodes, thus the interactions at the contact between the organic film and the metal electrode must be appropriately included into the modeling approach. As two different material types are interfaced at the contact, the tunneling scheme outlined above for the transport within the organic layer must be augmented. In addition to the spatial overlap discussed above, the height of the tunnel barrier is refined by two factors: First, the relative position of the Fermi level at the electrode surface and of the molecular HOMO and LUMO states determines the majority carrier species, because the injection barrier is lower into the state with the smaller potential difference with respect to the Fermi level. Second, if the molecule adjacent to the electrode is charged, an image charge of opposite sign can be induced in the metal which stabilizes the injected charge and smoothes the injection barrier. As both factors are decisive for the transport characteristics, as well as for the (desired) carrier recombination in more complex organic light emitting diodes, modeling schemes for such devices typically include according terms.

Finally, case (d) combines electronic and thermal aspects in shuttling transport, which has to be investigated especially for flexible organic film devices. As in case (c) the underlying transport mechanism is tunneling between adjacent confined, dispersion-less electronic states and depends on the tunneling probability. For regularly arranged arrays of molecules the thermally induced molecular vibrations do not modify the mean intermolecular distance. Yet, the tunneling probability depends non-linearly on the intermolecular distance, thus on average over all thermally activated configurations the mean tunneling probability increases [166]. In addition, the geometry changes induced by the thermal vibrations lead to shifts of the molecular electron levels. Averaging over all configurations, a broadening of the otherwise sharp electronic levels is obtained and indicated by the shaded areas in the lower part of panel (d). In this simplified picture, the effect of thermal vibrations on the overall electronic structure of the film resembles the broadening of the electron density of states by the k dispersion in metals or semiconductors. Note, however, that case (d) is based on a volume effect and is caused by a superposition of systems, which differ geometrically in real space, but still have strongly confined electronic levels. With regard to contacts with external wiring the same aspects as in case (c) are important. As (d) couples electronic and thermal transport, additional terms must be added, which account for structural and vibrational asymmetries and match the phonon properties of both materials in addition to the electronic ones. For instance, instead of applying a bias voltage, also a temperature gradient can trigger a directed thermocurrent or a diode behavior. The classification in cases (a) to (d) focuses strongly on the locality or non-locality of the electronic states and reflects the degree of structural order within the electronically active part of the system only in part. Therefore, a two-dimensional (2D) representation is introduced in Fig. 3, which allows for a better correlation of transport mechanism and electronic and structural settings. Panel (a) of Fig. 3 sketches the dependence between a the system uniformity as geometric parameter, the degree of carrier localization as electronic parameter, and the different conductivity types. The electron localization has been discussed already in the context of the four different mechanisms, but the definition of a uniformity parameter requires some attention.

In continuous nanostructures, such as wires or tubes, a uniformity value of 1 corresponds to systems with a well-defined, often bulk-like local coordination of the atoms, whereas systems with low uniformity exhibit a variety of different bond lengths and angles. For quantification the width of the signals in the radial distribution function can be chosen. For regular, self-assembled arrays of molecules, uniformity regards the spacing between adjacent molecules, their relative orientation and their orientation with respect to a substrate material. Deviations from ideal uniformity occur for molecules with low internal symmetry, which have many geometric degrees of freedom during nucleation and growth of the film. The extreme case are liquid crystalline layers with long-range order, but short-range conformational disorder. Template effects by the substrate enhance uniformity, but low uniformity results if the substrate provides binding sites at a distance, which is incommensurate with the intermolecular spacing or if several suitable binding sites are present on the substrate surface. Uniformity in such systems may be quantified either by direct imaging techniques, or, in larger regular patches by measuring broadening effects in electron diffraction or vibrational spectra.

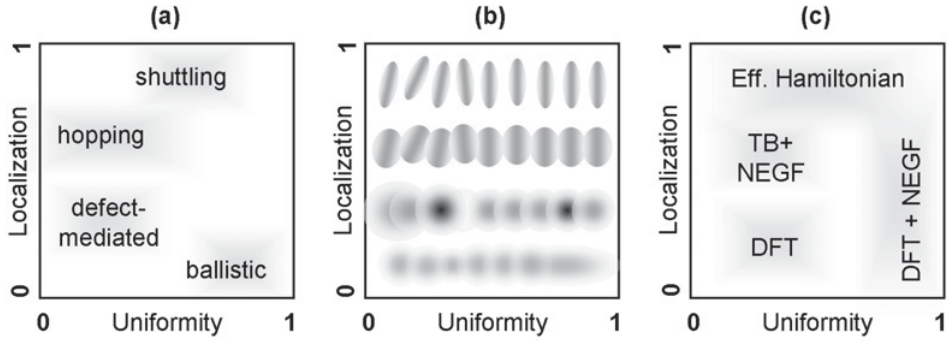

Fig. 3. Alternative 2D classification scheme for the transport mechanisms, geometrical features and simulation methods according to the degree of electron localization and structural (dis-)order. Panel (a) shows, where the different conduction mechanisms are located in this 2D graph; panel (b) depicts the implications for the system geometries and panel (c) describes, which of the simulation techniques introduced above is suited for which combination of electron localization and structural disorder.

Following the discussion of the four mechanisms, the electron localization increases from case (a) to case (d), hence ballistic, dopant-induced, hopping and shuttling transport are arranged from bottom to top. In real systems, cases (c) and (d) will overlap more strongly than indicated here, but in principle the shuttling-enhanced tunneling probability can enable transport also in systems with less spatial overlap than in classical hopping, case (c). Deviations from a uniform system structure are detrimental for (a) ballistic and (c) hopping conductance. In contrast, defect-induced electronic transport (b) relies on static structural imperfections, and shuttling (d) requires dynamic structure changes. Therefore, (a) and (c) occur towards the right part of the diagram, whereas (b) and (d) more on the left side.

The central panel of Fig. 3 visualizes simplified prototype structures. The structural uniformity is expressed by the relative size and alignment of the circular or ellipsoidal nano-objects, the electronic uniformity is coded by the depth of the greyscale, and the electron localization is depicted by color gradient and the width and overlap of the ellipsoids. Comparing panels (a) and (b) there remain prototype structures, the conductance properties of which are not covered by one of the mechanisms (a) to (d). In those cases the two nearest mechanisms both contribute have to be considered, and one arrives at a mixed conductance regime. Other possibilities include transport pathways which are not discussed here; superconductivity or ionic transport are two prominent examples.

The right panel gives a schematic overview of the methods introduced in the initial section and how they are ideally applied to the different transport regimes. In systems with an intrinsic band-based ballistic (a) or doping-enhanced (b) conductance a detailed knowledge of the particular electronic structure given by first-principles calculations provides the most precise insight, hence methods such as the DFT are best applicable there. As such approaches are free of material-specific parameters they are ideally suited to model the influence of dopants on the local atomistic and electronic structure. Likewise, they allow to identify interface-specific electronic states, image charge contributions and structural and chemical stabilities at the contact with the external leads. Supercells with appropriate interface model structures typically range up some hundred atoms, therefore very complex geometries and non-uniform have to be treated in separate calculations. Thus, the keyword DFT is located more in the lower right corner of the diagram.

Extensions to the transport properties by non-equilibrium Green's functions (NEGF) have been successfully applied to wires, but also to molecular electronics systems, where a single molecule with local electronic states is contacted by metallic leads. As the method is computationally more demanding than ground-state DFT, a higher system uniformity is required to keep the structure model small. Therefore, the corresponding entry is placed at the right border of the diagram.

The localized nature of molecular orbitals is ideally reflected in a tight-binding scheme. As DFT itself such approaches as the density-functional-based tight-binding are free of material-specific information derived from experimental data. The interaction parameters which enter such a scheme are stringently calculated from first principles. Nevertheless, the concomitant focus on the physics and chemistry of the valence electrons reduces the numerical effort considerably. In conjunction with specific algorithms for sparse matrix operations modern tight-binding schemes allow the treatment of larger and less uniform systems of up to several thousands of atoms with higher computational efficiency than full DFT. Even larger systems may be addressed in simplified tight-binding schemes with material-independent parameters, which provide the bridge to a classical treatment with effective Hamiltonians. Thus, tight-binding and extensions by the NEGF technique provide a valuable tool to study the transport in structurally more complex and electronically more localized systems than full DFT. The corresponding entry in the right panel of Fig. 3 is therefore placed towards the center of the diagram.

For larger and more disperse systems not each detail of the electronic structure will be of significance for the transport through the whole structure. Effective Hamiltonians neglect the particularities of the electronic structure and grasp only the relevant physical effects, hence they are ideally suited to model such situations in a qualitative manner. For experimentally well characterized setups, the model parameters can even be refined to reproduce the measurement. Alternatively, interaction, injection and tunneling parameters can be calculated from first principles in a similar way as the interaction parameters which enter the DF-based tight-binding scheme. In this way, effective Hamiltonian approaches help to close the size gap between nano-scale electronic structure methods and macro-scale electronics.

3 Quantum modelling – Ballistic, defect-induced and hopping conduction

Quantum-mechanical calculations are central to all investigations of electronic transport, in which nano-scale processes are of interest. Nano-scale in that context addresses both the specific length of the object under study and the time-scale on which the transport-relevant processes take place. For instance, for light to induce a photo current through a stack of molecules, the excited state must be long-lived enough to provide the possibility for the carriers to tunnel away along the chain of molecules or of otherwise localized states.

Figure 4 visualizes the different boundary condition settings one meets in a quantum-mechanical treatment of transport. Already a detailed knowledge of the ground state electronic levels within the electrically active part helps to identify spatially and energetically matching states. Panel (a) of Fig. 4 visualizes this simplest approach, which employs either the whole active element or a periodically repeated unit cell. For determining transport, contacts are introduced, and their influence on the stability and the electronic states at the interface of the initial state prior to transport can be calculated straightforwardly within a confined model system, which may be periodically repeated in a supercell approach, see panel (b). First investigations on the conductance properties of wires or tubes with the Landauer formula were based on results from such mean-field calculations, mostly DFT. Under the assumption of non-interacting electrons the conductance is obtained from [167,168]:

$$G = \frac{2e^2}{h} \sum_{k \epsilon R'} T_k = \frac{2e^2}{h} \sum_{k \epsilon R'} \left(\frac{1}{I_k} \sum_{k' \epsilon R'} I_{k'} |t_{kk'}|^2 \right). \tag{1}$$

There, the conductance G is calculated as sum over the transfer coefficients T_k per channel k, which can contribute to the transport. The values of T_k are calculated by summing the probability currents $I_{k'}$ of the involved states k', weighted by the square of the states' contribution to k, $t_{kk'}$, over all involved states k'. It was shown that all these quantities can be reexpressed in terms of ground states properties calculated with density-functional band-structure calculations in a pseudopotential formalism [168]. Modeling the system under transport conditions, however, implies that the structure can be subjected to an external bias. In that case, the two

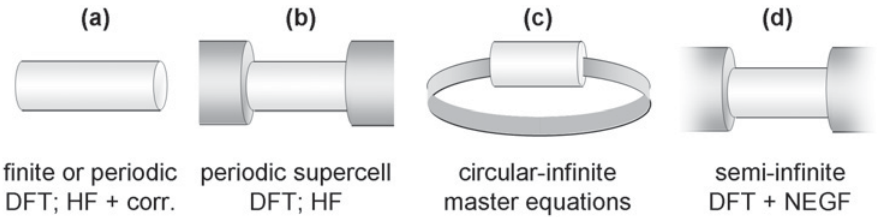

Fig. 4. Common boundary conditions for the quantum-based investigation of transport properties of nanostructures. Panel (a) depicts the molecular, cluster or repeated unit cell model structure usually employed in a ground-state study of the properties in the absence of an external bias. The additional interactions at the contact with the external wiring are covered in supercell or superstructure models of type (b). Boundary conditions which support the application of an external bias along the structure are of ring type (c) or, more commonly, base on a semi-infinite formulation for the contact material, as shown in panel (d).

contacts experience a potential difference, hence a periodic structure model such as (a) or (b) is not consistent with the electric boundary conditions. A ring-type geometry as shown in panel (c) has recently been suggested in a master equations approach. There, the potential difference applied to the central nanostructure has to be compensated by a reverse potential step within the larger metallic part, and with increasing ring size, the potential gradient within the metal becomes smaller and smaller. The standard solution, however, which is mostly applied in molecular electronics is to divide the metallic part into the explicitly treated contact region and a semi-infinite bulk part as indicated in panel (d). Such a setting allows to calculate the current J through the structure under applied bias in a non-equilibrium Green's function formulation for interacting electrons in the central part of the structure [169]:

$$J = \frac{ie}{2h} \int d\epsilon \left(tr([f_{\mathrm{L}}(\epsilon)\mathbf{\Gamma}^{\mathrm{L}} - f_{\mathrm{R}}(\epsilon)\mathbf{\Gamma}^{\mathrm{R}}](\mathbf{G}^r - \mathbf{G}^a)) + tr([\mathbf{\Gamma}^{\mathrm{L}} - \mathbf{\Gamma}^{\mathrm{R}}]\mathbf{G}^<) \right). \tag{2}$$

There, $f_{\mathrm{L}}(\epsilon)$ and $f_{\mathrm{R}}(\epsilon)$ are the Fermi-Dirac distribution functions in the left (L) and right (R) leads and $\mathbf{\Gamma}^{\mathrm{L/R}}$ are the transition rates between central structure and left/right leads. $\mathbf{G}^a$, $\mathbf{G}^r$, and $\mathbf{G}^<$ are the advanced, retarded and lesser GFs, which reflect the bias voltage dependence of the electronic states of the central structure and the associated current. In equilibrium the two leads are at equal (chemical) potential with $f_{\mathrm{L}}(\epsilon) = f_{\mathrm{R}}(\epsilon) = f_{\mathrm{eq.}}(\epsilon)$. In that case the lesser GF for transport in the central part reduces to $\mathbf{G}^< = -f_{\mathrm{eq.}}(\epsilon)(\mathbf{G}^r - \mathbf{G}^a)$, i.e. there is no zero current.

As Eq. (2) is quite complex, simplifications have been derived under the assumption of symmetric leads and/or of non-interacting electrons within the central structure. One thus arrives at Dyson equations to calculate $\mathbf{G}^<$, $\mathbf{G}^a$, and $\mathbf{G}^r$ in the intermediate region. With the resulting expressions, the current can be formulated in a more compact form as

$$J = \frac{e}{h} \int d\epsilon [f_{\mathrm{L}}(\epsilon) - f_{\mathrm{R}}(\epsilon)] tr(\mathbf{G}^a \mathbf{\Gamma}^{\mathrm{R}} \mathbf{G}^r \mathbf{\Gamma}^{\mathrm{L}}), \tag{3}$$

where the transition rates can be calculated from the hopping matrix between lead and central structure and the surface GF of the lead. A more detailed description of this procedure is given, e.g. in Ref. [170]. The present formalism and variants of it have been implemented in several quantum mechanical codes [60,144,171] and applied to systems ranging from metallic wires to arrays of $\pi-$stacked molecules. The number of investigated systems has increased tremendously in recent years, hence the present review can not cover all relevant literature, but rather focuses on a selection of investigations.

Since the observation of reproducible conductance jumps in mechanically controllable break junction experiments [172] nanoscale noble metal wires and point contacts have attracted numerous theoretical investigations to elucidate the correlation of structural, electronic and conductance properties. A strong dependence of the atomistic structure of gold nanowires on the

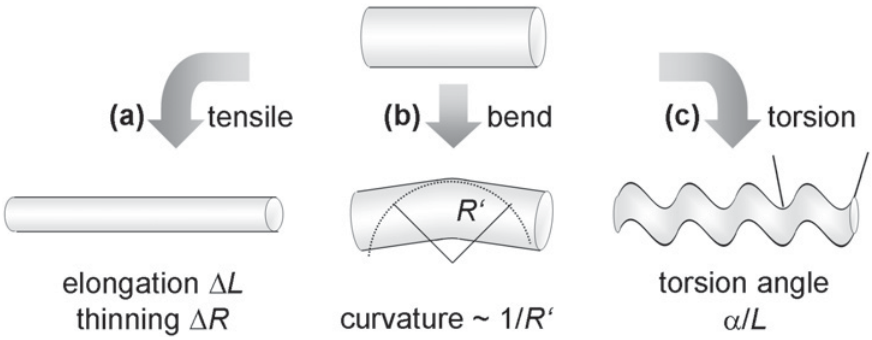

Fig. 5. Deformation modes exerted on nanowires as nano-scale leads for addressing devices on nanoscopic length scales. (a) Tensile stress induces thinning, (b) bending beyond a critical radius of curvature, R', leads to local atomic relaxations. Torsional strain, (c) is more complex as it can lead either to local or overall relaxations in addition to thinning or to switching between local minima of a structure if the torsion is commensurate with the structure.

preparation conditions could be attributed to strain states within the wire [175]. Chiral structures are obtained for gold, if the preparation conditions set the wires under tensile stress; otherwise, non-chiral, bulk-like structures are preferred [6]. Thus, also the vibrational properties deviate from the ones of bulk gold [176]. As the observed chiral structures are only local minima on the energy hypersurface, further thinning to monoatomic chains occurs [177]. For such monoatomic wires, observed deviations from the ideally quantized conductance could be correlated with an inhomogeneous distribution of bond lengths [178].

A synopsis of early work on the thinnest, monoatomic wires is given in ref. [179]. In excellent agreement with experimental in-situ transmission electron microscope measurements recent ground-state DFT calculations have shown that the crossover between quantized and continuum conductance sets on beyond a conductance of 10 G_0, where G_0 is the conductance quantum [1]. As the noble metals are non-magnetic, magnetic impurities have been introduced and the influence on the conductance properties were investigated. Landauer-type calculations find that the frozen spin conductance is slightly reduced if a nickel atom resides on a bridge position between two gold atoms, while a substitutional nickel atom does not influence the ideal conductance of gold [35]. Doping gold nanowires with other noble or near-noble metals such as silver or palladium allows tailoring the conductance properties of the gold wires, because the lower d electron density of the 4d metals reduces the tendency of gold towards surface crowding and reduces the internal stresses within the wire [17]. Via the structure-conductance relationship described above, the desired number of conductance channels can be settled. In this way, gold and other noble or near-noble metals can be employed either as functional element by itself or as nanoscale wiring for contacting other, e.g. molecular electronics setups.

In this context, the correlation between the number and symmetry of the conductance channels in gold nanowires and the strain state of the wire has inspired further studies on the influence of various deformations on the current transmitted through nanowires. A second motivation was provided by theoretical findings that conformation changes lead to significant conductance modifications in molecular electronics [184]. Figure 5 visualizes the geometries which may be encountered when thin metallic wires are employed for contacting other structures such as carbon nanotubes, semiconductor nanowires or electronically or optically active molecules. Tensile strain, depicted in panel (a), leads to wire thinning, as discussed above, and finally to rupture. Wires from ductile materials may also be bent up to a critical curvature quantified by the radius R' as indicated in panel (b) before major atom displacements or reconstructions occur [47]. Finally, such wires may also experience a torsional deformation (c), which is usually quantified by a critical torsion angle per unit length, see e.g. [173,174]. All these deformations have recently been studied for wires of another metallic conductor, the binary compound molybdenum sulfide. As shown by scanning tunneling spectroscopy in conjunction with DFT calculations, chains made of $(Mo_3S_3)_\infty$ exhibit electronic states at the Fermi level,

which give rise to metallic bonding [180]. The wires consist of a core of alternatingly stacked molybdenum triangles, which is surrounded by a shell of sulfur atoms. By DFT calculations the metallic states could be assigned to the metal core, whereas the sulfide shell is insulating. Thus, cross-talk between adjacent wires is hindered, because the inter-wire contacts are purely sulfur-based. As the structures observed by the scanning probe technique indicated a high flexibility of the wires, identified as $(Mo_3S_3)_\infty$, the deformations and their influence on the conductivity were investigated by DFT-based transport calculations with the NEGF method. As long as the elastic regime is maintained, bending does not change the metallic conductance of the wire. Already weak torsional deformations α/L of a few degrees per nm, however, lead to a reversible, structure-induced metal-insulator transition. An analysis of the band structure revealed that the effect is based on the symmetry reduction, which occurs during the torsion. Due to the loss of the mirror symmetry along the wire formerly crossing states of different symmetry fall into the same symmetry class in the distorted wire. The resulting forbidden crossing opens up a band gap of several tenths of an eV and switches the wire to a non-metallic state [47].

When such structures are contacted by gold nano-electrodes, the contact resistance can dominate the conductance properties. For instance, for electron transport in single- and double-wall CNTs contacted by metallic electrodes NEGF-Landauer calculations show that the symmetry of the contact region may induce blocking of a transport channel. For double-wall CNTs with both inner and outer shells being metallic, non-diagonal self energy contributions from the electrodes were obtained, which induce channel mixing. Hence, a simple addition of the individual shell conductances does not provide a realistic simulation of the experimentally observed current [181]. When molybdenum sulfide wires or wire segments are contacted by gold electrodes, however, no loss of conductance is obtained in NEGF-DFT calculations. The reason is a task sharing between molybdenum and sulfur atoms at the contact to gold. The sulfur atoms anchor the wire at some of the gold atoms on the surface of the electrode, whereas the central molybdenum core continues the gold wire structure and accounts for the metallic conductance. Contrary to systems from molecular electronics, where the contact has to accomplish both bonding and conductance, the current-carrying molybdenum levels are not affected by bonding to the electrode. As a consequence, the wire-electrode contact is almost ideally electron transparent [182].

The NEGF-DFT method has also been applied to systems with π-stacked aromatic molecules interfaced by two metal electrodes as indicated in Fig. 6 [185]. In such a geometry, no directed bonding between the molecules and the leads occurs, therefore there are no channels for ballistic carrier transfer. Instead, carrier injection occurs over a barrier, which comprises the potential step between the Fermi level of the lead and the involved molecular level, the image charge interaction induced in the polarizable metal by carriers localized on the first molecule(s) and the Coulomb repulsion, which blocks the transfer of like-charged carriers onto the same molecule. As decribed in Section 2 further transport occurs by tunneling or hopping of the carriers between the molecules, mediated by overlapping π states. Zero-bias calculations for the simplest test case, a benzene stack between two gold electrodes, indicate that the conductance decreases exponentially with increasing inter-electrode and inter-molecular spacings [166]. The same trends have recently been calculated for stacked oligothiophene molecules [113].

High-level, correlated ab-initio calculations on benzene oligomers have, moreover given evidence that the π-stacking interaction is short-ranged and limited to adjacent molecules [183]. Therefore, also simplified tight-binding approaches with hopping and on-site parameters from first-principles calculations have been successfully employed to describe electron and hole transport through π stacks of more complex organic molecules such as N-trimethyltriindole, a new p-type organic semiconductor, which grows with columnar order [186]. Internal reorganization energies within the stack and transfer integrals were estimated by gradient-corrected DFT calculations. As the HOMO energy coincides with the work function of gold (5.1 eV), the hole injection barrier is low and a high hole mobility of 0.4 $cm^2\ V^{-1}\ s^{-1}$ is obtained in very good agreement with the measurement. Another example is pentathienoacene, the thiophene equivalent of pentacene, for which the pronounced directionality of the transport along chains of π-stacked molecules and the influence of vibronic interactions has been extensively tested [187]. Among the wealth of investigations, a large amount of studies focuses on transport in DNA, where the inter-base transport has also been extensively studied with the help of various tight-binding-based Hamiltonians [127,156,163,188–191]. There, a gradual transition occurs to

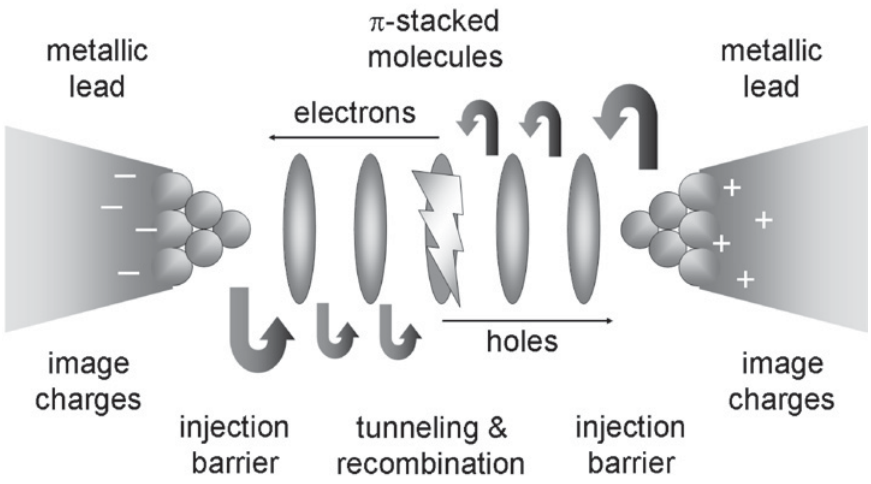

Fig. 6. Setup of a nano-device with a regular array of π-stacked aromatic molecules interfaced by metal electrodes. The processes and interactions relevant for electronic transport are indicated: holes and electrons as carriers have to overcome an injection barrier from the electrode to the first molecule(s), which combines tunneling from the Fermi level to the molecular state, image charge effects in the electrode and concomitant carrier accumulation on the first molecule(s); within the π stack carriers have to overcome intermolecular tunneling barriers and may recombine radiatively or non-radiatively.

classical models based on rate-theory with effective interaction and hopping parameters from experiment or electronic-structure calculation, which will be described in more detail in the following section.

4 Classical modelling – Rate equation and shuttling conduction

On the macroscopic side, classical Hamiltonians with a similar structure as the still electronic tight-binding treatment with effective transport parameters of the previous section are the bridge to the macroscopic scale, where the atomistic details vanish and the overall behavior of a real-scale circuitry are addressed by continuum simulations. The present discussion will focus on the micrometer length scale, where still the single physical processes can be distinguished qualitatively. As for the quantum-mechanics-based simulation, also here just a small part of the spectrum of available simulation techniques can be presented.

One model approach designed specially for the calculation of the behavior of organic light-emitting diodes is the MOLED code [133,134], which allows to describe the carrier distributions and densities as well as the potential landscape and the recombination probabilities in multiple organic layers, the so-called channel, between metallic electrodes. The approach is based on an effective 1-dimensional model, which can be applied, if the electrodes are planar and parallel to each other, if the π stack is homogeneously distributed and parallel to the electrodes, and if the distance between the electrodes sets the smallest length scale in the device. The key mechanisms in the underlying model Hamiltonian describe the carrier injection from the electrodes into the channel, the carrier transport via a phonon-assisted hopping process, and carrier recombination and emission of photons. The equations of motion for the carriers is described by a set rate equations, which give the evolution of the carrier concentration at each molecular site m:

$$\frac{dn_m}{dt} = \left(\frac{dn_m}{dt}\right)_{\text{inj}} + \left(\frac{dn_m}{dt}\right)_{\text{hop}} + \left(\frac{dn_m}{dt}\right)_{\text{rec}}, \tag{4}$$

where n represents electrons or holes and inj, hop, rec denote the changes due to injection, hopping and recombination. A considerable number of parameters such as molecular energy levels, electrode work functions and injection and hopping parameters allow a flexible adjustment of

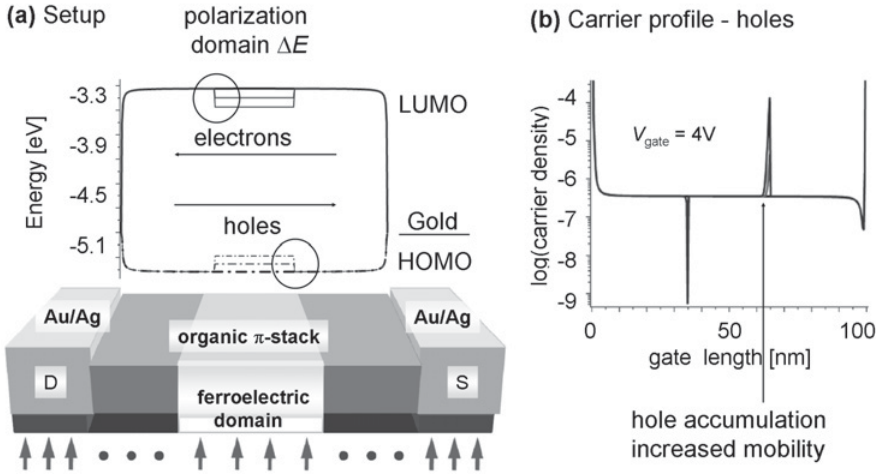

Fig. 7. Classical rate-equation simulation of transport in an organic field effect transistor. Panel (a) depicts the device setup (bottom) and the energies of the electronic levels involved in the transport (top). The simulated density profile of the majority carrier, holes, is shown in panel (b) as a function of the device geometry for an applied gate voltage of 4V.

the to the specific composition of the metal-organic-metal structure. Their proper choice is the main task in setting up the simulation. Recent efforts focused on a device composed of quaterthiophene, depicted in the central part of Fig. 1, as channel material and gold electrodes [113,192,193]

Within the channel, hole and electron transport are limited to the HOMO and LUMO levels of the organic molecules, which are taken from experiment or from electronic structure calculation. The levels change with the applied bias voltage and the carrier accumulation; near the electrode with correction terms for image charges and polarization. Far from the electrodes a homogeneous charge distribution within the molecules is assumed, hence localization by polarons is neglected. A high-level treatment of polaron interactions has been achieved in a path integral formalism [194], which is, however too detailed for an implementation in the present effective Hamiltonian formalism. The hopping parameter can be reexpressed in an atomic basis as sum over the Kohn-Sham matrix elements between the HOMO and LUMO levels on the adjacent molecules. For quaterthiophene (QT) it exhibits the exponential decay with increasing intermolecular distance discussed already for benzene stacks in section 3. The kinetics follows the carrier mobility observed in other organo-electronic setups, e.g. a Poole-Frenkel law, which determines the effective hopping frequency.

Parameters, which enter the transmission coefficient of the carrier injection from the electrodes are the contact area, the metal-molecule distance and the density of states at the Fermi level and the Fermi level itself. Geometric considerations give the first parameter, the others are conveniently obtained from electronic-structure calculations for the electrode surface. In the classical rate equation approach, carrier recombination depends only on the local electric field and carrier densities. Fig. 7 depicts the simulation setup for such an array of QT molecules, the π-stacked organic layer, interfaced by gold source (S) and drain (D) electrodes in the bottom of panel (a). The energy levels involved in carrier transport, i.e. the Fermi levels of the electrodes and the HOMO and LUMO levels of QT are shown in the diagram above the sketch of the device. As the Fermi energy is close to the HOMO level, hole injection from the left electrode is favorable, and panel (b) shows the distribution of the hole density inside the device. The hole enrichment close to the left electrode is due to a stabilization by the attractive image charge term. The depletion close to the right electrode reflects both enhanced recombination with injected electrons and the influence of the image charge term for electrons, which is repulsive for holes.

The additional features in the center of the channel show the effect of gating. As QT molecules are strongly polarizable by electric fields along the long direction of the molecule, a gate voltage can be applied perpendicular to the QT film, i.e. perpendicular to the source-drain direction. Such a polarization changes the HOMO and LUMO levels as indicated in the diagram and provides local attractors for holes and electrons. If the size of the gated area is small, the carrier localization leads to enhanced recombination rates, whereas the larger gated area shown in Fig. 7 features enhanced mobilities. As the schematic representation of the device suggests, gating may be achieved not only by an additional electric contact, but also by switching the surface polarity of a ferroelectric material in an external elastic field [192,193] or at the domain wall of a ferroic material [23]. In contrast to the active $(Mo_3S_3)_\infty$-based switch described above, such an element could be designed as sensor to monitor environment-induced changes, even aging of the substrate material.

Finally, the thermally induced motion of the organic material also influences the transport. Vibrational level broadening, the distance dependence of transfer integrals and conformation changes are effects commonly investigated to cover the correlation of electronic transport and the temperature of the system. Generalizing first-principles data for the ground state to thermal excitations, the electron or hole transfer between neighboring conducting polymer strands or oligomers was found to depend strongly on the charge-resonance integral and on the reorganization energy due to geometric relaxation. [195]. Geometry changes are also the central issue in studies of transport through DNA [196,197], carbon nanotubes [198], nanowires [177,199] or through benzoquinone derivatives [112], where the temperature dependence of the transfer integrals is estimated by classical molecular dynamics for the mean inter-molecular arrangement. The observed memory effect obtained with benzoquinone derivatives can be explained by showing that the OFF state is dominated by interface limited phenomena and the ON state more likely depends on bulk transport. On this basis it is suggested that control over molecular parameters has a large potential for the design of more efficient resistive molecular memories. If the influence temperature is limited to level broadening, convolution with a Gaussian profile may suffice [200].

A more simplistic recent model represents the molecules as structure-less, cylindrical and deformable nanoshafts positioned between two flat-walled, structure-less and ideally conducting electrodes. Carrier injection is achieved by bending the outermost shafts towards the electrodes until the critical distance for tunneling to the shaft is reached. Likewise, carrier transport occurs by shuttling, i.e. by bending adjacent shafts towards each other until hopping sets in [201]. In that setting the equation of motion for the carriers is only determined by the continuum elastics background of the oscillating nanoshafts and by the symmetry of the boundary conditions. For the symmetric model no zero-bias current is obtained, because thermally induced shuttling occurs in both directions with equal probability. In the asymmetric case, the model also yields the thermally induced current without external electrical bias, if the two electrodes are for instance at different temperature.

5 Challenges – Outlook

Potential for further developments exists in several directions: First, all methods outlined in the last two sections still experience extensions to cover the physics more appropriately or to include additional effects. Second, with the increased availability of parallel computing capacity improvements concerning more suitable algorithms and an efficient numerical implementation are demanded. And last but not least, the interplay of quantum-mechanics-based calculations and classical simulations towards a multi-scale modeling of transport is mostly mediated by parameter transfer, but a stringent, concurrent formulation bridging length and time scales is still to be developed.

Concerning the first topic, recent extensions focus on the inclusion of screening effects in the Coulomb blockade regime. A scheme has been devised to calculate the addition energy (difference between ionization and affinity levels) from NEGF-DFT data including also the image charge contribution. When applied to the transport simulation with the standard test

case of a benzene molecule aligned parallel to two planar gold electrodes the agreement with measured conductance data is noticeably improved [202]. Other attempts focus on applying a time-dependent formulation of current density functional theory to include also many-body effects into the simulation of the transport process [203–206]. Even external baths can be added to include the influence of external effects such as the temperature into so-called stochastic time-dependent current density functional theory, yet the approach is still computationally demanding [207]. Other challenges concerning the methodology itself have been elaborated in a recent review [83]; they mainly concern the case of molecules weakly bound to the electrodes, as mostly encountered in hopping transport. An improved approach, which includes exchange-correlation corrections is derived from current density functional theory. Open questions address the steady state limit, the dependence on a non-constant bias voltage, memory effects in the time-dependent Kohn-Sham potential and further effects of strong correlations between the electrons. Numerical improvements have mostly concentrated on matrix algorithms with better numerical stability or better parallelization properties [100,171].

Finally, standard concurrent schemes for embedding quantum mechanical regions into a classically treated background are well established to investigate the steady-state geometric and electronic features of complex nanostructures. There have been successful studies which focus on the intramolecular charge transfer in complex biomolecules such as the DNA. For instance, the mechanism of photolyase-catalyzed DNA repair has recently been elucidated by such QM/MM simulations and the active site of the protein could be localized [162]. Even different repair paths could be investigated and their importance for the repair process was weighted in this way [155]. Such calculations interfacing quantum and classical world can greatly assist the modern drug design, but a generalization to large-scale transport is still to come. The ingredients of such a scheme doubtlessly include a parameter-free electronic structure method, which yields the electronic states of the components and the local changes in the contact regions, plus a classical scheme to account for external effects such as thermally induced vibrations, electric, magnetic or elastic fields and the appied bias voltage. The boundary conditions at the interface between quantum and classical treatment have to be extended by terms which account for electrical polarizations as response to the external fields. Most challenging, however, are the different time scale involved in electronic, atomistic and molecular rearrangements. A proper concurrent treatment will have to include detailed averaging and refinement steps which are expectedly more complex than existing procedures in purely classical multi-scale methods [208,209].

The authors gratefully acknowledge support by the DFG via Priority Programme 1157 and the Research Unit FOR 520 and by the BMBF via the “Pakt für Forschung und Innovation”.

References

1. Y. Kurui, Y. Oshima, M. Okamoto, K. Takayanagi, Phys. Rev. B **79**, 165414 (2009)
2. C. He, P. Zhang, Y.F. Zhu, Q. Jiang, J. Phys. Chem. C **112**, 9045 (2008)
3. J.A. Torres, Sci. Tech. Adv. Mater. **8**, 186 (2007)
4. S. Dag, E. Durgun, S. Ciraci, Phys. Rev. B **69**, 121407 (2004)
5. P. Sen, O. Gülseren, T. Yildirim, I. Batra, S. Ciraci, Phys. Rev. B **65**, 235433 (2002)
6. E. Tosatti, S. Prestipino, S. Köstlmeier, A. Dal Corso, F. Di Tolla, Science **291**, 288 (2001)
7. T. Ando, H. Matsumura, T. Nakanishi, Physica B **323**, 44 (2002)
8. S. Agrawal, M.S. Raghuveer, R. Ramprasad, G. Ramanath, IEEE Trans. Nanotech. **6**, 722 (2007)
9. J. Kotakoski, A.V. Krasheninnikov, K. Nordlund, Phys. Rev. B **74**, 245420 (2006)
10. G. Kim, B.W. Jeong, J. Ihm, Appl. Phys. Lett. **88**, 193107 (2006)
11. A.N. Enyashin, S. Gemming, G. Seifert, Nanotechnology **18**, 245702 (2007)
12. T. Markussen, R. Rurali, A.P. Jauho, M. Brandbyge, Phys. Rev. Lett. **99**, 076803 (2007)
13. R. Rurali, T. Markussen, J. Sune, M. Brandbyge, A.P. Jauho, Nano Lett. **8**, 2825 (2008)
14. H. Peelaers, B. Partoens, F.M. Peeters, Physica E **40**, 2169 (2008)
15. M. Schreiber, S. Gemming, Comp. Phys. Commun. **169**, 57 (2005)
16. H. Li, K.M. Liew, X.Q. Zhang, J.X. Zhang, X.F. Liu, X.F. Bian, J. Phys. Chem. B **112**, 15588 (2008)

17. S. Gemming, G. Seifert, M. Schreiber, Phys. Rev. B **69**, 245410 (2004)
18. S. Gemming, M. Schreiber, Z. Metallkd. **94**, 238 (2003)
19. D. Qian, W.K. Liu, Q. Zheng, Comp. Meth. Appl. Mech. Eng. **197**, 3291 (2008)
20. P.V. Avramov, P.B. Sorokin, A.S. Fedorov, D.G. Fedorov, Y. Maeda, Phys. Rev. B **74**, 245417 (2006)
21. A. Smogunov, A. Dal Corso, E. Tosatti, Phys. Rev. B **78**, 014423 (2008)
22. B. Hope, A. Horsfield, Phys. Rev. B **77**, 094442 (2008)
23. J. Seidel, L.W. Martin, Q. He, Q. Zhan, Y.H. Chu, A. Rother, M.E. Hawkridge, P. Maksymovych, P. Yu, M. Gajek, et al., Nature Mater. **8**, 229 (2009)
24. U. Schwingenschloegl, C. Schuster, EPL **86**, 27005 (2009)
25. K. Janicka, J.P. Velev, E.Y. Tsymbal, Phys. Rev. Lett. **102**, 106803 (2009)
26. R. Pentcheva, W.E. Pickett, Phys. Rev. Lett. **102**, 107602 (2009)
27. J. Lee, A.A. Demkov, Phys. Rev. B **78**, 193104 (2008)
28. Z.S. Popovic, S. Satpathy, R.M. Martin, Phys. Rev. Lett. **101**, 256801 (2008)
29. R. Pentcheva, W.E. Pickett, Phys. Rev. B **78**, 205106 (2008)
30. M.J. Han, J. Yu, J. Kor. Phys. Soc. **53**, 1074 (2008)
31. U. Schwingenschloegl, C. Schuster, Ann. Phys. **17**, 525 (2008)
32. J.M. Albina, M. Mrovec, B. Meyer, C. Elsaesser, Phys. Rev. B **76**, 165103 (2007)
33. P.R. Willmott, S.A. Pauli, R. Herger, C.M. Schlepuetz, D. Martoccia, B.D. Patterson, B. Delley, R. Clarke, D. Kumah, C. Cionca, et al., Phys. Rev. Lett. **99**, 155502 (2007)
34. S. Gemming, G. Seifert, Acta Mater. **54**, 4299 (2006)
35. Y. Miura, R. Mazzarello, A. Dal Corso, A. Smogunov, E. Tosatti, Phys. Rev. B **78**, 205412 (2008)
36. L. Ke, M. van Schilfgaarde, T. Kotani, P.A. Bennett, Nanotechnology **18**, 095709 (2007)
37. J. Kim, N. Kim, S. Lee, T. Kang, Semicon. Sci. Tech. **21**, 647 (2006)
38. A. Smogunov, A. Dal Corso, E. Tosatti, Phys. Rev. B **73**, 075418 (2006)
39. A. Calzolari, N. Marzari, I. Souza, M. Nardelli, Phys. Rev. B **69**, 035108 (2004)
40. D. Csontos, H. Xu, Phys. Rev. B **67**, 235322 (2003)
41. H.M. Moghaddam, S.A. Ketabi, N. Shahtahmasebi, J. Phys.: Condens. Matter **19**, 116211 (2007)
42. Y.F. Li, B.R. Li, H.L. Zhang, Nanotechnology **20**, 225202 (2009)
43. J. Taylor, H. Guo, J. Wang, Phys. Rev. B **63**, 245407 (2001)
44. G. Fagas, J.C. Greer, Nano Lett. **9**, 1856 (2009)
45. Z. Qian, R. Li, S. Hou, Z. Xue, S. Sanvito, J. Chem. Phys. **127**, 194710 (2007)
46. J. Burki, C. Stafford, X. Zotos, D. Baeriswyl, Phys. Rev. B **60**, 5000 (1999)
47. I. Popov, S. Gemming, S. Okano, N. Ranjan, G. Seifert, Nano Lett. **8**, 4093 (2008)
48. A. Terasawa, T. Tada, S. Watanabe, Phys. Rev. B **79**, 195436 (2009)
49. G. Wei, H. Yi-Bin, Z. Yu-Yang, D. Shi-Xuan, G. Hong-Jun, Chin. Phys. B **18**, 2502 (2009)
50. C. Xiao-Chun, Y. Jun, Z. Yan-Hong, X. Ying, Acta Phys. Sin. **58**, 3064 (2009)
51. B. Wang, Y. Yu, L. Zhang, Y. Wei, J. Wang, Phys. Rev. B **79**, 155117 (2009)
52. M.M. Fadlallah, C. Schuster, U. Schwingenschloegl, T. Wunderlich, S. Sanvito, J. Phys.: Condens. Matter **21**, 315001 (2009)
53. D.E. Petersen, S. Li, K. Stokbro, H.H.B. Sörensen, P.C. Hansen, S. Skelboe, E. Darve, J. Comp. Phys. **228**, 5020 (2009)
54. S. Hou, Y. Chen, X. Shen, R. Li, J. Ning, Z. Qian, S. Sanvito, Chem. Phys. **354**, 106 (2008)
55. H. Aghaie, M.R. Gholmi, M.D. Ganji, M.M. Taghavi, Curr. Appl. Phys. **9**, 367 (2009)
56. P. Zhao, D.S. Liu, S.J. Xie, Phys. Lett. A **372**, 5811 (2008)
57. R. Stadler, V. Geskin, J. Cornil, J. Phys.: Condens. Matter **20**, 374105 (2008)
58. M.J. Ford, R.C. Hoft, A.M. McDonagh, M.B. Cortie, J. Phys.: Condens. Matter **20**, 374106 (2008)
59. H. Aghaie, M.R. Gholami, M. Monajjemi, M.D. Ganji, Physica E **40**, 2965 (2008)
60. A. Pecchia, G. Penazzi, L. Salvucci, A. Di Carlo, New J. Phys. **10**, 065022 (2008)
61. H. Zeng, H.F. Hu, J.W. Wei, W.W. Yang, P. Peng, Eur. Phys. J. A **43**, 19 (2008)
62. M.D. Ganji, F. Nourozi, Physica E **40**, 2606 (2008)
63. Z. Qian, S. Hou, R. Li, Z. Shen, X. Zhao, Z. Xue, J. Comp. Theo. Nanosci. **5**, 671 (2008)
64. R. Stadler, V. Geskin, J. Cornil, Adv. Functional Mater. **18**, 1119 (2008)
65. P. Bai, E. Li, K.T. Lam, O. Kurniawan, W.S. Koh, Nanotechnology **19**, 115203 (2008)
66. K. Stokbro, J. Phys.: Condens. Matter **20**, 064216 (2008)
67. R. Li, J. Zhang, S. Hou, Z. Qian, Z. Shen, X. Zhao, Z. Xue, Chem. Phys. **336**, 127 (2007)
68. F.D. Novaes, A.J.R. da Silva, A. Fazzio, Brazilian J. Phys. **36**, 799 (2006)
69. P. Jelinek, R. Perez, J. Ortega, F. Flores, Surf. Sci. **566**, 13 (2004)

70. A. Pecchia, A. Di Carlo, Rep. Prog. Phys. **67**, 1497 (2004)
71. Y. Xue, S. Datta, M. Ratner, Chem. Phys. **281**, 151 (2002)
72. P. Damle, A. Ghosh, S. Datta, Chem. Phys. **281**, 171 (2002)
73. J. Mozos, P. Ordejon, M. Brandbyge, J. Taylor, K. Stokbro, Nanotechnology **13**, 346 (2002)
74. D. Waldron, L. Liu, H. Guo, Nanotechnology **18**, 424026 (2007)
75. P. Bose, A. Ernst, I. Mertig, J. Henk, Phys. Rev. B **78**, 092403 (2008)
76. C. Heiliger, M. Czerner, B.Y. Yavorsky, I. Mertig, M.D. Stiles, J. Appl. Phys. **103**, 07A709 (2008)
77. M. Czerner, B.Y. Yavorsky, I. Mertig, Phys. Rev. B **77**, 104411 (2008)
78. N. Papanikolaou, J. Opitz, P. Zahn, I. Mertig, Phys. Rev. B **66**, 165441 (2002)
79. M. Wierzbowska, A. Delin, E. Tosatti, Phys. Rev. B **72**, 035439 (2005)
80. N. Stojic, A. Dal Corso, B. Zhou, S. Baroni, Phys. Rev. B **77**, 195116 (2008)
81. S. Bellucci, P. Onorato, Eur. Phys. J. B **47**, 385 (2005)
82. J.S. Evans, O.A. Vydrov, T. Van Voorhis, J. Chem. Phys. **131**, 034106 (2009)
83. M. Koentopp, C. Chang, K. Burke, R. Car, J. Phys.: Condens. Matter **20**, 083203 (2008)
84. D. Akinwande, J. Liang, S. Chong, Y. Nishi, H.S.P. Wong, J. Appl. Phys. **104**, 124514 (2008)
85. N.Y. Kim, P. Recher, W.D. Oliver, Y. Yamamoto, J. Kong, H. Dai, Phys. Rev. Lett. **99**, 036802 (2007)
86. C. Lee, J. Cho, J. Ihm, K. Ahn, Phys. Rev. B **69**, 205403 (2004)
87. W. Ren, F. Xu, J. Wang, Nanotechnology **19**, 435402 (2008)
88. R. Avriller, S. Roche, F. Triozon, X. Blase, S. Latil, Mod. Phys. Lett. B **21**, 1955 (2007)
89. T. Markussen, R. Rurali, M. Brandbyge, A.P. Jauho, Phys. Rev. B **74**, 245313 (2006)
90. P. Cain, M. Schreiber, Eur. Phys. J. Special Topics **161**, 249 (2008)
91. Y.Y. Zhang, J. Hu, B.A. Bernevig, X.R. Wang, X.C. Xie, W.M. Liu, Phys. Rev. Lett. **102**, 106401 (2009)
92. D. Hughes, P. Ballone, Phys. Rev. B **77**, 245312 (2008)
93. S. Akhanjee, J. Rudnick, Phys. Rev. Lett. **99**, 236403 (2007)
94. V.Z. Cerovski, Phys. Rev. B **75**, 113101 (2007)
95. M. Schreiber, M. Ottomeier, J. Phys.: Condens. Matter **4**, 1959 (1992)
96. B. Kramer, A. Kawabata, M. Schreiber, Phil. Mag. B **65**, 595 (1992)
97. H. Grussbach, M. Schreiber, Phys. Rev. B **51**, 663 (1995)
98. H. Sakai, Y. Takane, J. Phys. Soc. Jpn. **75**, 054711 (2006)
99. R. Chen, A.I. Hochbaum, P. Murphy, J. Moore, P. Yang, A. Majumdar, Phys. Rev. Lett. **101**, 105501 (2008)
100. A. Stotland, R. Budoyo, T. Peer, T. Kottos, D. Cohen, J. Phys. A **41**, 262001 (2008)
101. D.P. Wang, D.E. Feldman, B.R. Perkins, A.J. Yin, G.H. Wang, J.M. Xu, A. Zaslavsky, Sol. State Commun. **142**, 287 (2007)
102. N.P. Stepina, E.S. Koptev, A.V. Dvurechenskii, A.I. Nikiforov, Microelectronics J. **40**, 766 (2009)
103. D. Cohen, Phys. Rev. B **75**, 125316 (2007)
104. C. Mudry, P. Brouwer, A. Furusaki, Phys. Rev. B **62**, 8249 (2000)
105. Y.X. Li, H.W. Lee, H.Y. Choi, Phys. Lett. A **372**, 6424 (2008)
106. B. Dong, X.L. Lei, N.J.M. Horing, Phys. Rev. B **77**, 085309 (2008)
107. W.z. Wang, Phys. Rev. B **76**, 115114 (2007)
108. R.E. Chandler, A.J. Houtepen, J. Nelson, D. Vanmaekelbergh, Phys. Rev. B **75**, 085325 (2007)
109. R. Zitko, J. Bonca, Phys. Rev. Lett. **98**, 047203 (2007)
110. R. Aguado, D. Langreth, Phys. Rev. Lett. **85**, 1946 (2000)
111. K. Kang, M. Cha, S. Yang, Phys. Rev. B **56**, R4344 (1997)
112. S. Di Motta, E. Di Donato, F. Negri, G. Orlandi, D. Fazzi, C. Castiglioni, J. Am. Chem. Soc. **131**, 6591 (2009)
113. K. Morawetz, S. Gemming, R. Luschtinetz, T. Kunze, P. Lipavsky, L.M. Eng, G. Seifert, V. Pankoke, P. Milde, Phys. Rev. B **79**, 085405 (2009)
114. Z. Lu, C. Lo, C. Huang, Y. Yuan, M. Dharma-Wardana, M. Zgierski, Phys. Rev. B **72**, 155440 (2005)
115. R. Michalitsch, P. Lang, A. Yassar, G. Nauer, F. Garnier, Adv. Mater. **9**, 321 (1997)
116. B.B. Schmidt, M.H. Hettler, G. Schoen, Phys. Rev. B **77**, 165337 (2008)
117. T. Cramer, S. Krapf, T. Koslowski, J. Phys. Chem. C **111**, 8105 (2007)
118. Y. Asai, J. Phys. Chem. B **107**, 4647 (2003)
119. X.L. Liu, H. Xu, C.S. Deng, S.S. Ma, Physica B **383**, 226 (2006)
120. L. Mühlbacher, J. Ankerhold, C. Escher, J. Chem. Phys. **121**, 12696 (2004)

121. D.J. Mowbray, C. Morgan, K.S. Thygesen, Phys. Rev. B **79**, 195431 (2009)
122. D. Nozaki, Y. Girard, K. Yoshizawa, J. Phys. Chem. C **112**, 17408 (2008)
123. A.N. Andriotis, M. Menon, Appl. Phys. Lett. **89**, 132116 (2006)
124. D. Csontos, H. Xu, J. Phys.: Condens. Matter **14**, 12513 (2002)
125. K.H. Khoo, J.R. Chelikowsky, Phys. Rev. B **79**, 205422 (2009)
126. W. Wilson, Phys. Rev. **127**, 1549 (1962)
127. E. Conwell, *Polarons and transport in DNA*, Top. Curr. Chem. **237** (2004)
128. R.G. Sarmento, E.L. Albuquerque, P.D. Sesion, Jr., U.L. Fulco, B.P.W. de Oliveira, Phys. Lett. A **373**, 1486 (2009)
129. Z. Qu, D.w. Kang, Y. Li, W. Liu, D.s. Liu, S.j. Xie, Phys. Lett. A **372**, 6013 (2008)
130. S.C. Wang, P.C. Li, H.C. Tseng, Physica A **387**, 5159 (2008)
131. F.A.B.F. de Moura, M.L. Lyra, E.L. Albuquerque, J. Phys.: Condens. Matter **20**, 075109 (2008)
132. D. Porath, G. Cuniberti, R. Di Felice, *Charge transport in DNA-based devices*, Top. Curr. Chem. **237** (2004)
133. D. Berner, H. Houili, W. Leo, L. Zuppiroli, Phys. Stat. Sol. A **202**, 9 (2005)
134. H. Houili, E. Tutis, H. Lutjens, M. Bussac, L. Zuppiroli, Comp. Phys. Commun. **156**, 108 (2003)
135. H. Liu, W. Ni, J. Zhao, N. Wang, Y. Guo, T. Taketsugu, M. Kiguchi, K. Murakoshi, J. Chem. Phys. **130**, 244501 (2009)
136. D.B. de Lima, J. del Nero, J. Comp. Theo. Nanoscience **5**, 1445 (2008)
137. I.S. Kristensen, D.J. Mowbray, K.S. Thygesen, K.W. Jacobsen, J. Phys.: Condens. Matter **20**, 374101 (2008)
138. Y.X. Zhou, F. Jiang, H. Chen, R. Note, H. Mizuseki, Y. Kawazoe, J. Chem. Phys. **128**, 044704 (2008)
139. S.H. Ke, H.U. Baranger, W. Yang, J. Comp. Theo. Nanoscience **3**, 819 (2006)
140. S. Ke, H. Baranger, W. Yang, J. Chem. Phys. **123**, 114701 (2005)
141. J. Seminario, L. Yan, Int. J. Quantum Chem. **102**, 711 (2005)
142. Y. Jang, S. Hwang, Y. Kim, S. Jang, W. Goddard, J. Am. Chem. Soc. **126**, 12636 (2004)
143. A. Patnaik, H. Setoyama, N. Ueno, J. Chem. Phys. **120**, 6214 (2004)
144. K. Stokbro, J. Taylor, M. Brandbyge, J. Mozos, P. Ordejon, Comp. Mater. Sci. **27**, 151 (2003)
145. E. Pop, S. Sinha, K.E. Goodson, Proc. IEEE **94**, 1587 (2006)
146. G. Horowitz, J. Mater. Res. **19**, 1946 (2004)
147. A. Ghosh, P. Damle, S. Datta, A. Nitzan, MRS Bull. **29**, 391 (2004)
148. P. Krstic, D. Dean, X. Zhang, D. Keffer, Y. Leng, P. Cummings, J. Wells, Comp. Mater. Sci. **28**, 321 (2003)
149. H. Chen, C. Hsu, J. Phys. Chem. A **109**, 11989 (2005)
150. R. Hoffmann, Acc. Chem. Res. **4**, 1 (1971)
151. A. Clayton, G. Scholes, K. Ghiggino, M. PaddonRow, J. Phys. Chem. **100**, 10912 (1996)
152. A. Chatterjee, W. Holley, Int. J. Quantum Chem. **39**, 709 (1991)
153. P. DiGennaro, G. Sello, M. Termini, J. Theo. Biol. **181**, 359 (1996)
154. S. Priyadarshy, S. Risser, D. Beratan, J. Phys. Chem. **100**, 17678 (1996)
155. J. Rak, A. Voityuk, M. Michel-Beyerle, N. Rösch, J. Phys. Chem. A **103**, 3569 (1999)
156. M. Zhao, Y. Xia, Y. Ma, M. Ying, X. Liu, L. Mei, Phys. Lett. A **300**, 421 (2002)
157. J. Rak, A. Voityuk, N. Rösch, J. Mol. Struct. – Theochem **488**, 163 (1999)
158. A. Voityuk, N. Rösch, J. Phys. Chem. A **101**, 8335 (1997)
159. J. Rak, A. Voityuk, N. Rösch, J. Phys. Chem. A **102**, 7168 (1998)
160. J. Hahn, M. Michel-Beyerle, N. Rösch, J. Mol. Modeling **4**, 73 (1998)
161. J. Hahn, M. Michel-Beyerle, N. Rösch, J. Phys. Chem. B **103**, 2001 (1999)
162. F. Masson, T. Laino, U. Röthlisberger, J. Hutter, Chem. Phys. Chem. **10**, 400 (2009)
163. D. Reha, W. Barford, S. Harris, Phys. Chem. Chem. Phys. **10**, 5436 (2008)
164. A.S.P. Gomes, C.R. Jacob, L. Visscher, Phys. Chem. Chem. Phys. **10**, 5353 (2008)
165. A. Amini, A. Harriman, J. Photochem. Photobiol. C **4**, 155 (2003)
166. M. Mine, T. TsuTsui, E. Miyoshi, Jpn. J. Appl. Phys. **47**, 8033 (2008)
167. R. Landauer, Philos. Mag. **21**, 863 (1970)
168. H.J. Choi, J. Ihm, Phys. Rev. B **59**, 2267 (1998)
169. Y. Meir, N.S. Wingreen, Phys. Rev. Lett. **68**, 2512 (1992)
170. S. Datta, Superlatt. Microstruct. **28**, 253 (2000)
171. I. Rungger, S. Sanvito, Phys. Rev. B **78**, 035407 (2008)
172. C.J. Muller, J.M. van Ruitenbeek, L.J. De Jongh, Phys. Rev. Lett. **69**, 140 (1992)

173. T. Cohen-Karni, L. Segev, O. Srur-Lavi, S.R. Cohen, E. Joselevich, Nature Nanotech. **1**, 36 (2006)
174. N. Geblinger, A. Ismach, E. Joselevich, Nature Nanotech. **3**, 199 (2008)
175. Q. Pu, Y. Leng, P.T. Cummings J. Am. Chem. Soc. **130**, 17907 (2008)
176. J. Zhou, J. Dong, Phys. Rev. B **75**, 155423 (2007)
177. J.A. Torres, E. Tosatti, A. Dal Corso, F. Ercolessi, J.J. Kohanoff, F.D. Di Tolla, J.M. Soler, Surf. Sci. **426**, L441 (1999)
178. F. Picaud, V. Pouthier, C. Girardet, E. Tosatti, Surf. Sci. **547**, 249 (2003)
179. E. Tosatti, Solid State Commun. **135**, 610 (2005)
180. J. Kibsgaard, A. Tuxen, M. Levisen, E. Laegsgaard, S. Gemming, G. Seifert, J.V. Lauritsen, F. Besenbacher, Nano Lett. **8**, 3928 (2008)
181. N. Ranjan, R. Gutierrez, S. Krompiewski, G. Cuniberti, Mol. Phys. Rep. **40**, 125 (2004)
182. I. Popov, A. Pecchia, S. Okano, N. Ranjan, A. Di Carlo, G. Seifert, Appl. Phys. Lett. **93**, 083115 (2008)
183. T.P. Tauer, C.D. Sherrill, Appl. Phys. Lett. **109**, 10475 (2005)
184. M. Tsukada, K. Tagami, K. Hirose, N. Kobayashi, J. Phys. Soc. Jpn. **74**, 1079 (2005)
185. Y. Zhu, T.H. Lin, Q.F. Sun, Comm. Theo. Phys. **40**, 369 (2003)
186. E.M. Garcia-Fruto, E. Gutierrez-Puebla, M. Angeles Monge, R. Ramirez, P. de Andres, A. de Andres, B. Gomez-Lor, Org. Electronic **10**, 643 (2009)
187. E.G. Kim, V. Coropceanu, N.E. Gruhn, R.S. Sanchez-Carrera, R. Snoeberger, A.J. Matzger, J.-L. Bredas, J. Am. Chem. Soc. **129**, 13072 (2007)
188. Y.J. Ye, R.S. Chen, A. Martinez, P. Otto, J. Ladik, Solid. St. Commun. **112**, 139 (1999)
189. H-Y. Zhang, X.Q. Li, P. Han, X.Y. Yu, Y.J. Yan, J. Chem. Phys. **117**, 4578 (2002)
190. G. Cuniberti, L. Craco, D. Porath, C. Dekker, Phys. Rev. B **65**, 241314 (2002)
191. A. Ivanova, G. Jezierski, N. Rösch, Phys. Chem. Chem. Phys. **10**, 414 (2008)
192. S. Gemming, R. Luschtinetz, I. Chaplygin, G. Seifert, Ch. Loppacher, L.M. Eng, T. Kunze, C. Olbrich, Eur. Phys. J. Special Topics **149**, 145 (2007)
193. S. Gemming, R. Luschtinetz, W. Alsheimer, G. Seifert, Ch. Loppacher, L.M. Eng, J. Computer-Aided Mater. Des. **14**, 211 (2007)
194. S. Chiucchi, S. Fratini, Phys. Rev. B **79**, 035113 (2009)
195. G.R. Hutchison, M.A. Ratner, T.J. Marks, J. Am. Chem. Soc. **127**, 16866 (2005)
196. J.P. Lewis, J. Pikus, T.E. Cheatham, E.B. Starikov, H. Wang, J. Tomfohr, O.F. Sankey, Phys. Stat. Sol. (b) **233**, 90 (2002)
197. P.B. Woiczikowski, T. Kubar, R. Gutierrez, R.A. Caetano, G. Cuniberti, M. Elstner, J. Chem. Phys. **130**, 215104 (2009)
198. J.R. Lukes, H. Zhong, J. Heat Transf. **129**, 705 (2007)
199. S. Ciraci, A. Buldum, I.P. Batra, J. Phys.: Condens. Matter **13**, R537 (2001)
200. L.M. Andersson, O. Inganaes, Org. Electronics **8**, 423 (2007)
201. K. Morawetz, S. Gemming, R. Luschtinetz, L.M. Eng, G. Seifert, A. Kenfack, New J. Phys. **10**, 103014 (2008)
202. R. Stadler, V. Geskin, J. Cornil, Phys. Rev. B **79**, 113408 (2009)
203. H. Eschrig, G. Seifert, P. Ziesche, Sol. Stat. Commun. **56**, 777 (1985)
204. E. Runge, E.K.U. Gross, Phys. Rev. Lett. **52**, 997 (1984)
205. G. Vignale, W. Kohn, Phys. Rev. Lett. **77**, 2037 (1996)
206. S.K. Ghosh, A.K. Dhara, Phys. Rev. A **38**, 1149 (1988)
207. M. Di Ventra, R. D'Agosta, Phys. Rev. Lett. **98**, 226403 (2007)
208. J. Kundin, M. Radke de Cuba, S. Gemming, H. Emmerich, Physica D **238**, 117 (2009)
209. M. Radke de Cuba, H. Emmerich, S. Gemming, Eur. Phys. J. Special Topics. **149**, 43 (2007)